Published in final edited form as:
Chem Res Toxicol. 2007 August ; 20(8): 1200–1210. doi:10.1021/tx700121j.

Bulge Migration of the Malondialdehdye OPdG DNA Adduct When Placed Opposite a Two-Base Deletion in the $(CpG)_3$ Frameshift Hotspot of the *Salmonella typhimurium hisD3052* Gene

Yazhen Wang[†], **Nathalie C. Schnetz-Boutaud**[‡], **Sam Saleh**[‡], **Lawrence J. Marnett**[‡], and **Michael P. Stone**[*,†]
Departments of Chemistry and Biochemistry, Institute of Chemical Biology, Center in Molecular Toxicology, A. B. Hancock, Jr., Memorial Laboratory for Cancer Research, Vanderbilt-Ingram Cancer Center, Vanderbilt University, Nashville, Tennessee 37235

Abstract

The OPdG adduct N^2-(3-oxo-1-propenyl)dG, formed in DNA exposed to malondialdehyde, was introduced into 5′-d(ATCGCXCGGCATG)-3′•5′-d(CATGCCGCGAT)-3′ at pH 7 (X = OPdG). The OPdG adduct is the base-catalyzed rearrangement product of the M_1dG adduct, 3-(*β*-D-ribofuranosyl) pyrimido[1,2-*a*]purin-10(3*H*)-one. This duplex, named the OPdG-2BD oligodeoxynucleotide, was derived from a frameshift hotspot of the *Salmonella typhimuium hisD3052* gene and contained a two-base deletion in the complementary strand. NMR spectroscopy revealed that the OPdG-2BD oligodeoxynucleotide underwent rapid bulge migration. This hindered its conversion to the M_1dG-2BD duplex, in which the bulge was localized and consisted of the M_1dG adduct and the 3′-neighbor dC [Schnetz-Boutaud, N. C., Saleh, S., Marnett, L. J., and Stone, M. P. (2001) *Biochemistry 40*, 15638−15649]. The spectroscopic data suggested that bulge migration transiently positioned OPdG opposite dC in the complementary strand, hindering formation of the M_1dG-2BD duplex, or alternatively, reverting rapidly formed intermediates in the OPdG to M_1dG reaction pathway when dC was placed opposite from OPdG. The approach of initially formed M_1dG-2BD or OPdG-2BD duplexes to an equilibrium mixture of the M_1dG-2BD and OPdG-2BD duplexes was monitored as a function of time, using NMR spectroscopy. Both samples attained equilibrium in ~140 days at pH 7 and 25 °C.

* To whom correspondence should be addressed. Phone: (615) 322−2589. Fax: (615) 322−7591. E-mail: michael.p.stone@vanderbilt.edu..
[†]Department of Chemistry.
[‡]Department of Biochemistry.

Supporting Information **Available:** Chemical shifts of nonexchangeable protons for the OPdG- and M_1dG-2BD duplexes (Tables S1 and S2, respectively) and chemical shifts of exchangeable protons for the OPdG- and M_1dG-2BD duplexes (Tables S3 and S4, respectively). This material is available free of charge via the Internet at http://pubs.acs.org.

Introduction

The exocyclic guanine adduct M_1dG [1] [3-(2′-deoxy-*β*-D-*erythro*-pentofuranosyl)pyrimido[1,2-α]purin-10(3*H*)-one] arises in DNA from multiple sources. One source is exposure to malondialdehyde (MDA), a toxic and mutagenic metabolite produced by lipid peroxidation and prostaglandin biosynthesis (for a review, see refs 1 and 2). In aqueous solution, MDA exists as *β*-hydroxyacrolein. It reacts with DNA as a bis-electrophile to form M_1dG (3–7). Alternatively, the M_1dG adduct arises as a consequence of oxidative damage to DNA, resulting in the formation of base propenals that subsequently transfer their oxopropenyl group to dG (8) (Scheme 1). The base propenals are significantly more potent than MDA in forming M_1dG (9).

The M_1dG adduct has been identified in DNA from rodent (10) and human (11,12) tissue samples, as have other exocyclic purine lesions (13–16), suggesting their presence in vivo. The levels of M_1dG adducts in DNA have been quantitated by mass spectrometric (17,18), postlabeling (19,20), and immunochemical (21) techniques. This endogenously formed adduct is the most abundant exocyclic adduct present in human DNA (18–20,22). It has also been detected at low levels in human urine (23). The low urinary levels of M_1dG likely reflect metabolic conversion to the 6-oxo-M_1dG derivative (24). M_1dG is an efficient premutagenic lesion in *Escherichia coli* (25,26), mammalian (26), and human (27) cells. Thus, the M_1dG adduct is anticipated to mediate human carcinogenesis.

The M_1dG adduct is stable in nucleotides and single-stranded DNA at neutral pH. Under basic conditions, it converts to the N^2-(3-oxo-1-propenyl)dG (OPdG) derivative. In contrast, when M_1dG is placed at neutral pH into duplex DNA opposite dC, a spontaneous conversion to the OPdG derivative is facilitated. Upon denaturation of the duplex, M_1dG is regenerated (Scheme 2). Ring opening does not occur at neutral pH in duplex DNA if thymine is placed opposite from M_1dG. These observations suggested that dC in duplex DNA catalyzes the transformation of M_1dG to its ring-opened OPdG derivative (28). The ring opening of M_1dG as a nucleoside or in oligodeoxynucleotides is a reversible second-order reaction with hydroxide ion (29). The reverse ring closure mechanism involves rapid formation of protonated OPdG and 8-hydroxy-6,7-propenodG intermediates that slowly converts to M_1dG in a general acid-catalyzed reaction (30).

A refined structure was obtained for the OPdG adduct in 5′-d(ATCGCXCGGCATG)-3′•5′-d(CATGCCGCGCGAT)-3′ (X =OPdG) (31). This sequence contains the $d(CpG)_3$ frameshift mutation hotspot located in the *Salmonella typhimurium hisD3052* gene. The structure of the OPdG adduct embedded in this sequence was of interest because MDA, a small alkylating agent, induced frameshift mutations (32). In this structure, OPdG maintained stacking interactions with neighboring bases. It was not Watson–Crick hydrogen bonded. The cytosine complementary to OPdG was pushed toward the major groove but maintained partial stacking with its neighboring bases. The modified guanine remained in the *anti* conformation, while the OPdG 3-oxo-1-propenyl moiety was positioned in the minor groove of the duplex (31).

The frameshift mutations observed in vivo in *E. coli* and in COS-7 cells and associated with the $d(CpG)_3$ iterated repeat included −2 bp deletions (26). Thus, it was of interest to examine

[1]Abbreviations: MDA, malondialdehyde; M_1dG, 3-(*β*-D-ribofuranosyl)pyrimido[1,2-*a*]purin-10(3*H*)-one; OPdG, N^2-(3-oxo-1-propenyl)deoxyguanosine; PdG, 1,N^2-propano-dG; HO-PdG, 8-hydroxy-6,7-propenodeoxyguanosine; EDTA, ethylenediaminetetraacetic acid; HPLC, high-performance liquid chromatography; NOE, nuclear Overhauser enhancement; NOESY, two-dimensional NOE spectroscopy; COSY, correlation spectroscopy; DQF-COSY, double-quantum-filtered correlation spectroscopy; TPPI, time-proportional phase increment; 1D, one-dimensional; 2D, two-dimensional. A right superscript refers to the numerical position in the sequence starting from the 5′-terminus of chain A and proceeding to the 3′-terminus of chain A and then from the 5′-terminus of chain B to the 3′-terminus of chain B. C2, C5, C6, C8, C1′, C2′, C2″, etc., represent specific carbon nuclei. H2, H5, H6, H8, H1′, H2′, H2″, etc., represent protons attached to these carbons.

oligodeoxynucleotides containinga2bp (CpG) deletion opposite either M_1dG or OPdG. Additionally, replication bypass studies conducted in vitro suggested that DNA polymerase *β* induced two-base deletions when replicating past M_1dG in this iterated sequence derived from the *S. typhimuium hisD3052* gene. [2] Previous NMR structural studies examined the M_1dG adduct in the 5′-d($A^{-2}T^{-1}C^1G^2C^3X^4C^5G^6G^7C^8A^9T^{10}G^{11}$)-3′•5′-d($C^{12}A^{13}T^{14}G^{15}C^{16}C^{17}G^{18}C^{19}G^{20}A^{21}T^{22}$)-3′ sequence containing a 2 bp deletion in the complementary strand (Scheme 2), named the M_1dG-2BD oligodeoxynucleotide (33). In that freshly prepared sample, the two-base bulge in the M_1dG-2BD oligodeoxynucleotide was reported to be localized and consisted of M_1dG and the 3′-neighbor dC. The structure of the M_1dG-2BD duplex suggested that the bulged sequence lacked a cytosine properly positioned to facilitate opening of M_1dG and supported the conclusion that proper positioning of dC complementary to M_1dG is necessary for promotion of ring opening of the exocyclic adduct in duplex DNA (33). The structure of the M_1dG-2BD duplex was similar to that of the structural analogue 1,N^2-propanodeoxyguanosine (PdG) in the corresponding PdG-2BD duplex (34). The fixed position of the bulged bases in both instances suggested (33) that these exocyclic adducts did not facilitate bulge migration, a phenomenon first reported by Woodson and Crothers (35,36).

The NMR studies presented here examine the OPdG-2BD oligodeoxynucleotide, in which the OPdG adduct is placed opposite the two-nucleotide deletion (Scheme 1). In contrast to the M_1dG-2BD oligodeoxynucleotide (33), the OPdG-2BD oligodeoxynucleotide undergoes rapid bulge migration (35,36). This hinders its conversion to the M_1dG-2BD duplex (33). The data suggest that bulge migration transiently positions OPdG opposite dC in the complementary strand or, alternatively, reverts rapidly formed intermediates in the OPdG to M_1dG reaction pathway (30) when dC is placed opposite from OPdG. In contrast, the localized bulge in the M_1dG-2BD duplex consisting of the M_1dG adduct and the 3′-neighbor dC (33) hinders the conversion of M_1dG to OPdG that is catalyzed by the positioning of cytosine opposite from M_1dG (28,29). The addition of either M_1dG-2BD- or OPdG-2BD-containing samples to an equilibrium mixture was monitored as a function of time, using NMR spectroscopy. Both samples attained equilibrium, slightly favoring the M_1dG-2BD duplex, in ~140 days at pH 7 and 25 °C.

Materials and Methods

Oligodeoxynucleotide Synthesis

The unmodified oligodeoxynucleotide was synthesized by the Midland Certified Reagent Co. (Midland, TX) and purified by anion-exchange chromatography. M_1dG was synthesized, purified, and incorporated into oligodeoxynucleotides using either an older (37,38) or a more recently described and improved methodology (39). The extinction coefficients of the oligodeoxynucleotides were calculated on the basis of nearest-neighbor analysis and were 1.04×10^5 M^{-1} cm^{-1} for the M_1dG-modified strand 5′-d(ATCGCXCGGCATG)-3′ and 1.01×10^5 M^{-1} cm^{-1} for the complementary strand 5′-d(CATGCCGCGAT)-3′ (40). To prepare the OPdG-2BD duplex, the 13-mer containing the M_1dG adduct was combined with the 11-mer complementary strand at a 1:1 molar ratio in 0.1 M NaCl, 10 mM NaH_2PO_4, and 50 μM Na_2EDTA at pH 11.8. After 3 h at room temperature, the buffer was rapidly adjusted to pH 7.0. The M_1dG-2BD duplex was prepared as previously described (33). For spectroscopic examination of the nonexchangeable protons, the OPdG-2BD and M_1dG-2BD samples were then lyophilized and exchanged three times with D_2O and then suspended in 99.996% D_2O. Samples used for spectroscopic examination of exchangeable protons were suspended in a 9:1

[2]Riggins, J. N., and Marnett, L. J. (2001) Malondialdehyde-deoxyguanosine Adducts M_1dG and N^2 OPdG Block Replication by Human DNA Polymerase *β* and Induce Frameshift Mutations in Vitro, 222nd American Chemical Society National Meeting, Chicago, IL, Division of Chemical Toxicology, Collected Abstracts.

H_2O/D_2O mixture. The concentrations of both the OPdG-2BD and M_1dG-2BD duplex samples were 0.52 mM. The concentration of the unmodified duplex sample was 1.1 mM.

NMR Spectroscopy

^{1}H NMR spectra were recorded at 500.13 and 800.13 MHz. Chemical shifts were referenced to the water resonance. Phase sensitive NOESY spectra used for resonance assignments were recorded at 25 ± 0.5 °C using TPPI phase cycling with a mixing time of 250 ms. For examination of exchangeable protons, phase sensitive NOESY experiments were carried out using a field gradient Watergate pulse sequence for water suppression (41). The spectra were recorded at 10 ± 0.5 °C with a mixing time of 150 ms. These experiments were generally recorded with 512 real data points in the d_1 dimension and 2048 real data points in the d_2 dimension. A relaxation delay of 1.9 s was used for these experiments. The data were processed using FELIX (Accelrys, Inc., San Diego, CA) on Octane workstations (Silicon Graphics, Inc., Mountain View, CA). The data in the d_1 dimension were zero-filled to give a matrix of 2048 × 2048 real points. A skewed sine-bell square apodization function with a 90° phase shift and a skew factor of 1.0 was used in both dimensions.

Results

^{1}H Resonance Assignments of Nonexchangeable DNA Protons for the Unmodified 2BD Duplex

The unmodified 2BD duplex contained eight cytosines. These each exhibited sharp COSY cross-peaks arising from H5–H6 scalar couplings, shown in Figure 1A. Although there was spectral overlap arising from the iterated $C^1G^2C^3G^4C^5G^6$ repeat sequence, at 800 MHz it was possible to resolve resonances with slightly different chemical shifts. Thus, the C^3 H6 resonance was located at 7.35 ppm, slightly downfield of C^{17} H6, located at 7.36 ppm. The C^3 H5 resonance was located at 5.46 ppm, slightly upfield from the C^{17} H5 resonance, located at 5.49 ppm. The C^5 H6 resonance was located at 7.19 ppm, slightly upfield of the C^{19}H6 resonance located at 7.22 ppm. The C^8 H6 resonance was located at 7.28 ppm, slightly upfield of the C^{16} H6 resonance located at 7.31 ppm.

An expanded plot from the NOESY spectrum for the unmodified 2BD duplex, showing the sequential aromatic–anomeric proton connectivities, is also shown in Figure 2 A,B. The NOESY data were also characterized by sharp cross-peaks. The sequential NOE assignments were made using standard protocols (42, 43). The A^{-2} H1′ → T^{-1} H6 cross-peak was weak, reflecting fraying at the terminal A^{-2}•T^{22} base pair. The T^{22} H1′ resonance was located at 6.01 ppm. The T^{-1} H1′ resonance was located at 5.97 ppm, the C^1 H1′ resonance at 5.92 ppm, and the G^2 H1′ resonance at 5.94 ppm. In the 13-mer strand, this resulted in overlap of the T^{-2} H6 → T^{-1} H1′ and G^2 H1′ → C^3 H6, T^{-1} H1′ → C^1 H6 and C^1 H6 → C^1 H1′, and C^1 H1′ → G^2 H8 and G^2 H8 → G^2 H1′ NOESY cross-peaks. The C^3 H6 → C^3 H1′ cross-peak was partially superimposed upon the stronger C^3 H5 → C^3 H6 and C^{17} H5 → C^{17} H6 cross-peaks. The G^4 H8 resonance was located at 7.87 ppm, slightly downfield of G^{18} H8, located at 7.84 ppm. This caused the G^4 H8 → G^4 H1′ and G^{18} H8 → G^{18} H1′ cross-peaks to be superimposed. The G^4 H8 → C^5 H6 cross-peak overlapped with the G^{18} H8 → C^{19} H6 cross-peak, and the C^5 H6 → C^5 H1′ cross-peak overlapped with the C^{19} H6 → C^{19} H1′ cross-peak. The C^{19} H1′ resonance was located at 5.58 ppm, slightly downfield of G^{20} H1′, located at 5.45 ppm. The chemical shifts of the nonexchangeable protons are listed in Table S1 of the Supporting Information.

^{1}H Resonance Assignments of Exchangeable DNA Protons for the Unmodified 2BD Duplex

The far-downfield region of the NOESY spectrum showing the exchangeable resonances arising from the Watson–Crick base-paired imino protons is shown in Figure 3A. A complete

sequential connectivity was traced in the noniterated portion of the oligodeoxynucleotide duplex, from G^{6} N1H → G^{7} N1H → G^{15} N1H → T^{14} N3H → T^{10} N3H using standard protocols (44). The G^{11} N1H resonance was not observed, presumably due to fraying of the G^{11}•C^{12} terminal base pair, accompanied by rapid exchange with solvent. There were no unusual chemical shifts noted among this group of resonances. The imino resonance for the A^{-2}•T^{22} terminal base pair at the other end of the oligodeoxynucletoide duplex was also not observed, presumably due to rapid exchange with solvent. In the reiterated portion of the 2BD duplex, the imino resonance arising from T^{-1} N3H was also not observed, suggesting its rapid exchange with solvent. In addition, a broad resonance, assigned as one or more of the imino proton resonances arising from nucleotides G^{20}, G^{18}, G^{2}, and G^{4}, was observed at ~12.9 ppm. Consequently, the imino resonances from nucleotides T^{-1}, and nucleotides G^{20}, G^{18}, G^{2}, and G^{4}, located in the iterated repeat portion of the duplex, could not be unequivocally identified. The exocyclic N^{4} amino protons of cytosines exhibit longer lifetimes with respect to solvent exchange than the N3 imino protons. Inspection of the amino region of the ^{1}H NMR spectrum (Figure 3A) revealed the presence of resonances arising from hydrogen-bonded and non-hydrogen-bonded exocyclic amino protons of nucleotides C^{1}, C^{19}, C^{3}, and C^{5}. This indicated that on the NMR time scale, each of the nucleotides (C^{1}, C^{19}, C^{3}, and C^{5}) was involved in Watson–Crick hydrogen bonding with a deoxyguanosine in the complementary strand. Thus, the nucleotides in the complementary strand, G^{18}, C^{19}, and G^{20}, must be transiently forming Watson–Crick hydrogen bonds with C^{1}, G^{2}, C^{3}, G^{4}, and C^{5} in the parent strand, i.e., bulge migration (35) (see Scheme 2). No cross-peaks were observed between the hydrogen-bonded and non-hydrogen-bonded N^{4} exocyclic amino protons of C^{1} and deoxyguanosine imino protons. Furthermore, the chemical shift difference between the hydrogen-bonded and non-hydrogen-bonded amino protons of C^{1} was smaller than that observed for the other deoxycytosine residues, with the exception of terminal deoxycytosine residue C^{12}. This observation suggested that on the NMR time scale, nucleotides C^{1} and G^{2} were preferentially unpaired as compared to nucleotides G^{4} and C^{5}. In effect, the unmodified duplex was undergoing sequential fraying from the 5′-terminus of the 13-mer strand, extending into the duplex and involving the A^{-2}•T^{22}, T^{-1}•A^{21}, C^{1}•G^{20}, and G^{2}•C^{19} base pairs. The chemical shifts of the exchangeable protons are listed in Table S4 of the Supporting Information.

^{1}H Resonance Assignments of Nonexchangeable DNA Protons for the OPdG-2BD Duplex

As compared to those of the unmodified 2BD duplex, the resonances arising from the iterated $C^{1}G^{2}C^{3}G^{4}C^{5}G^{6}$ repeat sequence of the OPdG-2BD duplex exhibited better resolution. The eight cytosines each exhibited sharp COSY cross-peaks arising from H5–H6 scalar couplings, as shown in Figure 1 B.

The sequential NOE assignments shown in Figure 2 C,D were made using standard protocols (42, 43). No disruptions in sequential NOE connectivity were observed in either the modified stand or the complementary strand. In the modified 13-mer strand, the A^{-2} H1′ → T^{-1} H6, T^{-1} H6 → T^{-1} H1′, and T^{-1} H1′ → G^{2} H8 cross-peaks were weak, probably reflecting an increased level of fraying at terminal A^{-2}•G^{22} and T^{-1}•A^{21} base pairs. The C^{5} H1′ → G^{6} H8 cross-peak was also weak. In the complementary strand, the C^{16} H6 resonance was observed at 7.23 ppm while the C^{17} H6 resonance was observed at 7.30 ppm. The G^{15} H1′ resonance was observed at 5.73 ppm. This was slightly upfield of the C^{16} H1′ resonance. The G^{16} H1′ resonance was observed at 5.73 ppm. This caused both the G^{15} H1′ → C^{16} H6 and C^{16} H6 → C^{16} H1′ cross-peaks to be superimposed with the G^{18} H1′ → C^{19} H6 and C^{19} H6 → C^{19} H1′ cross-peaks. No unusual ^{1}H shifts were noted in this region of the spectrum. The C^{19} H1′ → G^{20} H8 and G^{20} H1′ → A^{21} H8 cross-peaks were weak, probably due to fraying at the terminal base pairs. The chemical shifts of the nonexchangeable protons are listed in Table S2 of the Supporting Information.

^{1}H Resonance Assignments of Exchangeable DNA Protons for the OPdG-2BD Duplex

The far-downfield region of the NOESY spectrum showing the exchangeable resonances arising from the Watson–Crick base-paired imino protons is shown in Figure 3 B. Significantly, it appeared substantially similar to the corresponding spectrum in Figure 3 A for the nonadducted 2BD duplex. For the non-reiterated portion of the duplex, sequential connectivity was traced from G^6 N1H → G^7 N1H → G^{15} N1H → T^{14} N3H → T^{10} N3H using standard protocols (44). There were no unusual chemical shifts noted among this group of resonances. The G^{11} N1H resonance was not observed, presumably due to fraying of the G^{11}•C^{12} terminal base pair, accompanied by rapid exchange with solvent. At the other end of the duplex, the imino resonance for the A^{-2}•T^{22} base pair was also not observed, suggesting rapid exchange with solvent. Additionally, the T^{-1} N3H resonance was not observed, presumably due to rapid exchange with solvent. A broad resonance, assigned as one or more of the imino proton resonances arising from nucleotides G^{20}, G^{18}, G^2, and X^4, was observed at ~12.9 ppm. Consequently, the imino resonances from nucleotides T^{-1}, and nucleotides G^{20}, G^{18}, G^2, and X^4, located in the iterated repeat portion of the duplex, could not be unequivocally identified. Inspection of the amino region of the ^{1}H NMR spectrum (Figure 3B) revealed weaker resonances arising from hydrogen-bonded and non-hydrogen-bonded exo-cyclic amino protons of nucleotides C^1, C^{19}, C^3, and C^5, as compared to the unmodified 2BD duplex (Figure 3A). This was attributed, in part, to the adducted sample being less concentrated but, more significantly, to slower bulge migration in the OPdG-2BD duplex as compared to the unmodified 2BD duplex, resulting in exchange broadening. Nevertheless, as in the unmodified 2BD duplex, on the NMR time scale, each of the nucleotides (C^1, C^{19}, C^3, and C^5) exhibited evidence of being involved in Watson–Crick hydrogen bonding with a deoxyguanosine in the complementary strand. Thus, the nucleotides in the complementary strand, G^{18}, C^{19}, and G^{20}, must be transiently forming Watson–Crick hydrogen bonds with C^1, G^2, C^3, X^4, and C^5, in the parent strand (see Scheme 2). No cross-peaks were observed between the hydrogen-bonded and non-hydrogen-bonded N^4 exocyclic amino protons of C^1 and deoxyguanosine imino protons. However, the chemical shift difference between the hydrogen-bonded and non-hydrogen-bonded amino protons of C^1 was now greater than that observed for C^1 in the unmodified 2BD duplex (Figure 3A), approaching that observed for the other deoxycytosine residues, with the exception of terminal deoxycytosine residue C^{12}. This suggested that on the NMR time scale, nucleotides C^1 and G^2 were paired more frequently than in the unmodified 2BD duplex; i.e., the presence of the OPdG lesion at X^4 resulted in somewhat more favorable paring of base pairs C^1•G^{20} and G^2•C^{19} than was the case in the unmodified 2BD duplex, but the OPdG-2BD duplex maintained a more rapid rate of bulge migration than did the M_1dG-2BD duplex, where the bulge was clearly localized at nucleotides X^4 and C^5. The chemical shifts of the exchangeable protons are listed in Table S4 of the Supporting Information.

Assignments of the OPdG Protons and NOEs between OPdG and DNA in the OPdG-2BD Duplex

The OPdG proton resonances were identified from a combination of NOESY and COSY experiments. Figure 4 shows the chemical shifts of OPdG protons and intermolecular NOEs between OPdG adduct protons and DNA. OPdG H8 was furthest downfield. At 8.96 ppm, it showed a strong NOE to OPdG H6 located at 7.95 ppm and a broad NOE to OPdG H7 located at 5.72 ppm. The OPdG H6 proton showed a broad NOE to OPdG H7. Six NOEs were observed between OPdG protons and DNA. All of these involved the adducted nucleotide X^4 and 3′-neighbor nucleotide C^5 in the modified strand. Both OPdG H8 and H6 exhibited NOEs to C^5 H5′ and C^5 H1′; OPdG H8 also exhibited a NOE to C^5 H4′ and X^4 H1′.

^{1}H Resonance Assignments of the M_1dG-2BD Duplex

The detailed NMR assignments of the M_1dG-2BD duplex were as previously reported (33). In contrast to the OPdG-2BD duplex and to the unmodified 2BD duplex, disruptions in sequential NOE connectivity were observed in both the modified and complementary strands. In the modified strand, the C^3 H1′ → X^4 H2 sequential NOE (X^4 H2 is the imidazole proton of M_1dG, corresponding to G^4 H8 in the unmodified nucleotide) was missing. In the complementary strand, the C^{17} H1′ → G^{18} H8 NOE was not observed. Spectral line broadening was localized adjacent to the M_1dG lesion. Line broadening was observed for the C^3 and C^5 H5 and H6 resonances. These were the 5′- and 3′-neighbors of the M_1dG lesion, respectively. In the complementary strand, line broadening was observed for C^{19} H5 and H6 (Figure 1 C). The assignments for the base imino protons of the M_1dG-2BD duplex showed an interruption in the sequential connectivity between imino protons at G^{18}, the base pair 5′ to the M_1dG lesion. No NOE connectivity was observed between G^{18} N1H and G^6 N1H, which localized the M_1dG adduct between base pairs C^5•G^{18} and G^6•C^{17}. The exocyclic M_1dG protons H6, H7, and H8 of M_1G were identified as the characteristic aromatic spin system. M_1dG H8 was observed at 8.4 ppm, M_1dG H7 at 5.8 ppm, and M_1dG H6 at 8.2 ppm. The following ^3J coupling constants for the M_1dG protons were measured in a DQF-COSY experiment: $^3J_{H6,H7} \sim 4$ Hz and $^3J_{H7,H8} \sim 7$ Hz. Figure 5 A shows chemical shift comparisons of cytosine protons H5 and H6, between the OPdG-2BD duplex and the unmodified 2BD duplex. No chemical shift perturbations were greater than 0.1 ppm except at position C^{16} H5 where a downfield shift of 0.24 ppm was observed. Figure 5 B shows chemical shift comparisons of cytosine proton H5–H6 cross-peaks, between the M_1dG-2BD duplex and the unmodified 2BD duplex. No chemical shift perturbations were greater than 0.1 ppm except at position C^5 in the modified strand and C^{19} in the complementary strand. A downfield shift of 0.44 ppm was observed for the C^5 H5 resonance, a downfield shift of 0.21 ppm for the C^5 H6 resonance, and a downfield shift of 0.17 ppm for the C^{19} H5 resonance.

Chemical Shift Comparisons between the OPdG-2BD and M_1dG-2BD Duplexes

Panels C and D of Figure 5 show chemical shift differences for the pyrimidine H5 and H6 or purine H8 and deoxyribose H1′ protons, comparing the OPdG-2BD and M_1dG-2BD duplexes. The ^{1}H chemical shifts of the non-reiterated base pairs G^6•C^{17}, G^7•C^{16}, C^8•G^{15}, A^9•T^{14}, T^{10}•A^{13}, and G^{11}•C^{12} were conserved in both duplexes. Significant chemical shift perturbations were observed for the reiterated base pairs associated with the two-nucleotide bulge, suggesting that the two-nucleotide bulge was differentially accommodated in the OPdG-2BD versus the M_1dG-2BD duplex. The biggest chemical shift difference between the OPdG-2BD duplex and the M_1dG-2BD duplex was 0.47 ppm, observed for the C^5 H5 resonance. Other significant shift changes were observed in the modified strand, 0.33 ppm for the C^1 H1′ resonance, 0.23 ppm for the G^2 H1′ resonance, 0.18 ppm for the C^3 H5 resonance, and 0.30 ppm for the C^5 H6 resonance. In the complementary strand, the G^{18} H8 resonance exhibited a 0.26 ppm shift.

Equilibrium of the OPdG-2BD and M_1dG-2BD Duplexes

The initially formed OPdG-2BD and M_1dG-2BD duplexes were not at equilibrium. The conversion of the OPdG-2BD duplex toward an equilibrium mixture of the M_1dG-2BD and OPdG-2BD duplexes was monitored as a function of time, by monitoring the COSY spectrum. Figure 6 monitors the ratio of resonance intensities from the C^1 H5–H6 COSY cross-peak of either OPdG or M_1dG as a function of time, beginning with freshly prepared OPdG-2BD or M_1dG-2BD duplexes. This cross-peak reflected the environment of the C^1•G^{20} base pair, located at the 5′-terminus of the iterated repeat sequence with respect to the OPdG-modified nucleotide X^4. Over a period of 140 days at 25 °C, the eight COSY cross-peaks arising from the OPdG-2BD duplex decreased in intensity and eight new cross-peaks corresponding to

formation of the M_1dG-2BD duplex appeared and grew in intensity. As noted above, for the OPdG-2BD duplex, the sequential connectivities in the reiterated region, T^{22} N3H → T^{-1} N3H → G^{20} N1H → G^{2} N1H → G^{18} N1H → G^{4} N1H → G^{6} N1H, were disturbed. As the OPdG duplex shifted toward the M_1dG-2BD duplex, these sequential connectivities appeared in the spectrum. At equilibrium, the M_1dG-2BD duplex was slightly favored. The equilibrium chemistry of a freshly prepared M_1dG-2BD duplex was also monitored. At equilibrium, the COSY spectrum of the initially prepared M_1dG-2BD duplex was identical to that of the OPdG-2BD duplex at equilibrium.

Discussion

Interest in the structure of the OPdG and M_1dG adducts embedded in the frameshift-prone *hisD3052*-iterated $(CG)_3$ repeat sequence arose from the observation that MDA induced frameshift mutations (32). The M_1dG and OPdG adducts are chemically distinct. One would predict that the biological processing of MDA- or base propenal-induced damage sites in DNA depends upon whether the damage exists as the exocyclic adduct M_1dG or as its OPdG rearrangement product. Site-specific mutagenesis experiments involving M_1dG (25) or its chemically stable analogue PdG (45), which cannot open to OPdG, indicated that PdG gave greater numbers of point mutations. Similarly, the acrolein-induced γ-hydroxyl-1,N^2-PdG adduct, which also underwent ring opening (46), was found to not be miscoding in vivo (47, 48).

It has not been possible to examine the M_1dG adduct with respect to structure in fully complementary DNA duplexes due to the fact that when placed opposite dC, it rapidly rearranges to the OPdG adduct (28). The saturated analogue 1,N^2-propanodG (PdG adduct) (49) was used by our laboratory (30,50–54) as well as by other laboratories (55–58) as a stable structural surrogate for exocyclic 1,N^2-dG adducts such as the M_1dG adduct and the acrolein γ-OH-PdG adduct. The PdG adduct reduced the thermal stability, transition enthalpy, and transition free energy of duplex DNA when positioned opposite dC or dA (59). When placed in the *hisD3052* gene-iterated CG repeat sequence at pH 5.8, PdG rotated about the glycosyl bond into the *syn* conformation, and the 3′-neighbor base pair existed in a mixture of Watson–Crick and Hoogsteen conformations (50). In a noniterated duplex at pH 5.2, only PdG and not its 3′-neighbor base pair rotated about the glycosyl bond into the *syn* conformation (54). Presumably, the *syn* conformation of the glycosyl bond relieves steric strain associated with incorporation of the 1,N^2-dG annelation product, which cannot participate in Watson–Crick hydrogen bonding, into the DNA duplex. In contrast, structural studies of the OPdG adduct in the fully complementary iterated repeat contained in the *hisD3052* oligodeoxynucleotide showed that it remained in the *anti* orientation about the glycosyl bond and oriented in the minor groove of the DNA duplex such that it did not interfere with Watson–Crick base pairing (31).

The iterated CG repeat contained in the *hisD3052* oligodeoxynucleotide is thought to be prone to frameshifts by slippage of either the template or the primer strand during DNA replication (60). The *hisD3052* mutation arose from the histidinol dehydrogenase gene of *S. typhimurium* by deletion of a cytosine induced by ICR-191 (61,62). It is reversed by additions and deletions that restore the reading frame but do not necessarily reverse the forward mutation (63). The most common reversion is a CG deletion in the reiterated sequence (64–67). The unmodified 2BD duplex and the M_1dG-2BD (33) and OPdG-2BD duplexes model the intermediate structures leading to two-base deletions.

Bulge Migration in the Unmodified 2BD Duplex

Woodson and Crothers (35) first characterized the phenomenon of bulge migration within iterated DNA sequences. Several lines of evidence suggest that formation of a two-nucleotide

bulge within the unmodified 2BD duplex was also accompanied by bulge migration. Significantly, a complete set of sequential NOE connectivities between nonexchangeable base aromatic and deoxyribose anomeric protons was observed (Figure 2 A,B). This observation was consistent with rapid migration of the two-nucleotide bulge in the *hisD3052* sequence such that on the NMR time scale, a set of sequential NOEs consistent with a right-handed duplex is observed for nucleotides C^1, G^2, C^3, G^4, C^5, and G^6. The presence of a localized two-nucleotide bulge on the NMR time scale would have predicted a break in these NOE connectivities, which was observed for the M_1dG-2BD duplex (33). In that instance, for the modified strand, the C^3 H1′ → M_1dG H2 sequential NOE (the imidazole proton of M_1dG, corresponding to G H8 in the unmodified nucleotide) was missing. In the complementary strand, the C^{17} H1′ → G^{18} H8 NOE was missing (33).

The observation that the eight cytosine H6–H5 COSY cross-peaks in Figure 1 A were well resolved corroborated the conclusion that the bulge migrated rapidly compared to the NMR time scale. In contrast, for the M_1dG-2BD duplex (Figure 1C), the localized bulge exhibited spectral line broadening adjacent to the M_1dG lesion, for the C^3 and C^5 cytosine H5 and cytosine H6 resonances, the 5′- and 3′-neighbors of the M_1dG lesion, respectively. In the complementary strand, line broadening was observed for C^{19} H5 and H6 (33).

The rapid bulge migration was also evident from the increased rate of solvent exchange of the dG N1H imino protons within the $(CG)_3$ iterated repeat sequence. In the non-reiterated portion of the bulged oligodeoxynucleotide, the dG N1H and dT N3H imino resonances arising from Watson–Crick base pairs G^6•C^{17}, G^7•C^{16}, C^8•G^{15}, A^9•T^{14}, and T^{10}•A^{13} were observed in the fardownfield region of the ^{1}H NMR spectrum, indicating that these base pairs had long lifetimes with respect to exchange of the hydrogen-bonded protons with solvent. For these base pairs in the non-reiterated portion of the bulged oligodeoxynucleotide, the normal patterns of NOEs between the dG N1H and dC N^4 exocyclic amino protons, characteristic of Watson–Crick base pairing, were observed in the ^{1}H NMR spectrum. In contrast, the dG N1H imino resonances arising from nucleotides G^{20}, G^2, G^{18}, and G^4 in the reiterated portion of the bulged oligodeoxynucleotide exhibited significant spectral line broadening associated with an increased rate of solvent exchange. However, for nucleotides C^1, C^{19}, C^3, and C^5 in the reiterated portion of the bulged oligodeoxynucleotide, NOEs between the dC N^4 exocyclic amino protons and the dG N1H protons of complementary deoxyguanosines, characteristic of individual Watson–Crick base pairs, could be assigned, indicating that transient Watson–Crick base pairing involving all four deoxycytosines in the reiterated portion of the duplex must be occurring. For the unmodified 2BD duplex, the T^{-1} N3H imino proton resonance arising from the T^{-1}•A^{21} base pair adjacent to the iterated repeat was not observed. Also, no cross-peaks were observed between the exocyclic N^4 amino protons of C^1 and guanine imino protons. In contrast, for the M_1dG-2BD duplex in which the two-nucleotide bulge was localized, an interruption in the sequential NOE connectivity between the dG N1H protons of adjacent base pairs was observed at G^{18}, the base pair 5′ to the M_1dG lesion, and no NOE was observed between G^{18} N1H and G^6 N1H, which localized the M_1dG adduct between base pairs C^5•G^{18} and G^6•C^{17} (33). For the M_1dG-2BD duplex, the T^{-1} N3H imino proton resonance arising from the T^{-1}•A^{21} base pair adjacent to the iterated repeat was observed. Also, cross-peaks from the N^4 exocyclic amine protons of C^1 to the G^{20} N1H imino proton were observed, indicating the presence of the C^1•G^{20} base pair (33).

Minor Groove Orientation of the OPdG Adduct in the OPdG-2BD Duplex

The pattern of NOEs observed between the OPdG moiety and the DNA in the OPdG-2BD duplex was consistent with a minor groove orientation of the OPdG adduct. The NOEs shown in Figure 4 involved X^4 H1′, and C^5 H1′, H4′, and H5′. These NOEs served to locate the OPdG moiety within the minor groove. Thus, the orientation of OPdG in the OPdG-2BD duplex was

similar to that in the fully complementary *hisD3052* oligodeoxynucleotide (31). However, the pattern of NOEs within the minor groove was different. In the fully complementary duplex, OPdG exhibited NOEs to minor groove protons in the complementary strand, e.g., C^{19} H1′, G^{20} H1′, G^{20} H4′, and G^{20} H5′ and H5″ (31).

Bulge Migration in the OPdG-2BD Duplex

The spectra of the OPdG-2BD duplex were similar to those from the unmodified 2BD duplex and differed from the spectra obtained for the M_1dG-2BD duplex (33). These observations suggested that formation of a two-nucleotide bulge within the OPdG-2BD duplex was also accompanied by bulge migration. The observation of a complete set of sequential NOE connectivities between nonexchangeable base aromatic and deoxyribose anomeric protons (Figure 2 C, D) was consistent with rapid migration of the two-nucleotide bulge such that on the NMR time scale, a set of sequential NOEs consistent with a right-handed duplex was observed for nucleotides C^1, G^2, C^3, X^4, C^5, and G^6. Eight well-resolved cytosine H6–H5 COSY cross-peaks were observed (Figure 1 B), also corroborating the conclusion that the bulge migrated rapidly on the NMR time scale. In the non-reiterated portion of the OPdG-2BD duplex, the dG N1H and dT N3H imino resonances from Watson–Crick base pairs G^6•C^{17}, G^7•C^{16}, C^8•G^{15}, A^9•T^{14}, and T^{10}•A^{13} were observed, indicating that these base pairs had long lifetimes with respect to exchange of the hydrogen-bonded protons with solvent. Furthermore, for these base pairs, the normal patterns of NOEs between the dG N1H and dC N^4 exocyclic amino protons, characteristic of Watson–Crick base pairing, were observed. In contrast, the dG N1H imino resonances arising from nucleotides G^{20}, G^2, G^{18}, and X^4 in the reiterated portion of the OPdG-2BD duplex exhibited spectral line broadening. For these nucleotides, the sequential NOEs between the dG N1H protons of adjacent base pairs and the NOEs between the dG N1H protons and the dC N^4 exocyclic amino protons, characteristic of individual Watson–Crick base pairs, could not be unequivocally assigned. In addition, the T^{-1} N3H imino proton resonance arising from the T^{-1}•A^{21} base pair adjacent to the iterated repeat was not observed, indicating that it also underwent solvent exchange at an increased rate (Figure 3B). The differential pattern of minor groove NOEs that was observed between the OPdG-2BD duplex and the fully complementary *hisD3052* duplex containing the OPdG adduct (31) was also consistent with bulge migration in the OPdG-2BD duplex. Thus, the rapid migration of the bulge precluded observation of NOEs to minor groove protons in the complementary strand but maintained the observation of NOEs to the 3′-neighbor nucleotide C^5 in the modified strand of the duplex.

The rapid rate of bulge migration is consistent with the observation that the OPdG adduct facilitates Watson–Crick base pairing, which was confirmed by Riggins et al. (30). Because OPdG does not interfere with Watson–Crick hydrogen bonding and is located in the minor groove, the location of the 2BD bulge is not localized. In contrast, M_1dG does interfere with Watson–Crick hydrogen bonding, and its accommodation in duplex DNA presumably requires its reorientation into the *syn* conformation about the glycosyl bond, similar to the case with the PdG adduct. Accordingly, the localization of the two-nucleotide bulge in the M_1dG-2BD duplex, involving the modified nucleotide X^4 and its 3′-neighbor C^5 (33), is favored.

Chemical Shift Differences among the Unmodified 2BD Duplex, the OPdG-2BD Duplex, and the M_1dG-2BD Duplex

The notion that the OPdG and M_1dG adducts existed in different environments within the iterated repeat sequence containing the two-nucleotide bulge was corroborated by examination of chemical shift effects (Figure 5). Only modest differences were observed when the chemical shifts for the cytosine H5 and H6 resonances of the unmodified 2BD duplex were compared to those of the OPdG-2BD duplex, consistent with the idea that these two duplexes behaved similarly. In contrast, a comparison of the unmodified 2BD duplex with the M_1dG-2BD duplex

showed a significant difference at nucleotide C5, the 3′-neighbor to the M_1dG-adducted nucleotide. Likewise, large chemical shift differences were observed when the OPdG duplex was compared with the M_1dG duplex. Significantly, these chemical shift differences were localized to the iterated repeat sections of the two bulged duplexes. Only minimal chemical shift differences were observed for the non-reiterated regions of the M_1dG-2BD duplex versus the OPdG-2BD duplex, consistent with the conclusion that the two bulged duplexes differed in the manners in which the respective adducts were accommodated within the iterated repeat sequence.

Differential Rates of Bulge Migration in the Bulged M_1dG-2BD and OPdG-2BD Duplexes Modulate the Rate at Which Equilibrium between M_1dG and OPdG Is Achieved

The differential rates of bulge migration in the M_1dG-2BD and OPdG-2BD duplexes affect the rate at which equilibrium between M_1dG and OPdG is achieved, as compared to that of fully complementary duplexes containing the M_1dG or OPdG adducts. For the fully complementary *hisD3052* duplex, the M_1dG adduct placed opposite dC rearranged to OPdG rapidly; its conversion was completed in minutes. For the M_1dG-2BD duplex, the two-base bulge was localized and consisted of M_1dG and the 3′-neighbor (33). As such, the M_1dG-2BD bulge lacks a hydrated cytosine positioned to facilitate opening of M_1dG (33); thus, at neutral pH, ring opening of M_1dG to OPdG occurs slowly in the M_1dG-2BD duplex. This study indicates that at 25 °C, equilibrium between M_1dG and OPdG, favoring M_1dG (33), was attained over a period of 140 days (Figure 6). This suggests that the localized bulge in the M_1dG-2BD duplex undergoes a slow migration. This was not recognized in the earlier studies (33), which were conducted using a freshly prepared M_1dG-2BD duplex. A slow migration of the bulge in the M_1dG-2BD duplex would transiently relocate M_1dG to a position opposite from nucleotide C^{19} in the complementary strand, which would facilitate ring opening of the OPdG adduct, via the mechanism proposed by Riggins et al. (29). Once the OPdG adduct forms at neutral pH, its more rapid bulge migration rate then slows the rate of its reversion back to the localized bulge in the M_1dG-2BD duplex. We conclude that the step in the formation of M_1dG, believed to be the dehydration of the initially formed 8-hydroxy-6,7-propenodG intermediate (30), is slow compared to bulge migration. Hence, it requires many days for the equilibrium involving OPdG and M_1dG in the OPdG-2BD and M_1dG-2BD duplexes to be attained.

Comparison to Other Oligodeoxynucleotides Containing Bulged Nucleotides

Previous studies examined oligodeoxynucleotides containing unpaired bases or bulges of various sequence contexts and length (68–75). Unpaired purines generally adopt intrahelical conformations in solution (74,76,77). For unpaired pyrimidines, both intrahelical (*7879*)and extrahelical conformations (*6980*)have been observed. The role of flanking DNA sequences in determining the conformation of bulged pyrimidines was demonstrated by studies demonstrating that bulged pyrimidines embedded in A•T tracts adopt an extrahelical conformation (70,81).

Structure–Activity Relationships

The M_1dG-induced frame-shift mutations observed in vivo in *E. coli* and in COS-7 cells, and associated with the $d(CpG)_3$ iterated repeat, include −2 bp deletions (26). These are consistent with the observation that frameshift mutations in the iterated CG repeat sequence of the *hisD3052* gene are typically −2 base deletions. These suggest mechanisms whereby the modified guanine and adjacent cytosine undergo transient dislocation during replication bypass (60,82). This work demonstrates rapid bulge migration within the iterated repeat sequence of the *hisD3052* gene containing the OPdG adduct. The occurrence of transient dislocation during replication could occur either prior to insertion of a nucleotide opposite M_1dG or, alternatively,

after nucleotide insertion and prior to extension (83). It could also involve dissociation or re-association with the replication complex.

In any case, relationships between DNA structure and dynamics, and the formation and accommodation of transient dislocation complexes during DNA replication, are anticipated to be polymerase-specific (84). Both M_1dG and OPdG block replication by the Klenow fragment of DNA polymerase I, with M_1dG being approximately 6-fold more blocking than OPdG (85). DNA polymerase β induces two-base deletions when replicating past M_1dG in this iterated d$(CpG)_3$ sequence derived from the *S. typhimuium hisD3052* gene. [2] However, the interactions of M_1dG and OPdG with various Y-family polymerases (86,87) remain to be determined and are likely to be crucial for understanding the mechanisms by which these lesions induce both frameshift and base pair substitution mutations in human cells. Significantly, structures of the *Sulfolobus solfataricus* P2 DNA polymerase IV (Dpo4) have been obtained for binary and ternary complexes with primer templates site-specifically modified with 1,N^2-ethenodeoxyguanosine (1,N^2-εdG) (88,89), an adduct that is structurally similar to M_1dG. The Dpo4 structures with the 1,N^2-εdG adduct suggest that it uses several mechanisms, including a variation of dNTP-stabilized misalignment, to generate frameshifts when it encounters the exocyclic DNA adduct (88).

Supplementary Material

Refer to Web version on PubMed Central for supplementary material.

Acknowledgment

Ms. Pamela Tamura and Dr. Ivan Kozekov synthesized the modified oligonucleotide. Mr. Markus Voehler assisted with the collection of NMR data. This work was supported by NIH Grants CA-55678 (M.P.S.) and CA-87819 (L.J.M.). Funding for the NMR spectrometers was supplied by Vanderbilt University, the Vanderbilt Center in Molecular Toxicology, Grant ES-00267, and by NIH Grant RR-05805. The Vanderbilt-Ingram Cancer Center is supported by NIH Grant CA-68485. Michael P. Stone grant RO1 CA-55678.

References

1. Marnett LJ. Lipid peroxidation-DNA damage by malondialdehyde. Mutat. Res 1999;424:83–95. [PubMed: 10064852]
2. Marnett LJ. Chemistry and biology of DNA damage by malondialdehyde. IARC Sci. Publ 1999;150:17–27. [PubMed: 10626205]
3. Basu AK, Essigmann JM. Site-specifically modified oligodeoxynucleotides as probes for the structural and biological effects of DNA-damaging agents. Chem. Res. Toxicol 1988;1:1–18. [PubMed: 2979705]
4. Marnett LJ, Basu AK, O'Hara SM, Weller PE, Rahman AFMM, Oliver JP. Reaction of malondialdehyde with guanine nucleosides: Formation of adducts containing oxadiazabicyclononene residues in the base-pairing region. J. Am. Chem. Soc 1986;108:1348–1350.
5. Seto H, Okuda T, Takesue T, Ikemura T. Reaction of malonaldehyde with nucleic acid. I. Formation of fluorescent pyrimido [1,2-*a*]purin-10(3H)-one nucleosides. Bull. Chem. Soc. Jpn 1983;56:1799–1802.
6. Seto H, Seto T, Takesue T, Ikemura T. Reaction of malonaldehyde with nucleic acid. III. Studies of the fluorescent substances released by enzymatic digestion of nucleic acids modified with malonaldehyde. Chem. Pharm. Bull 1986;34:5079–5085. [PubMed: 2436822]
7. Reddy GR, Marnett LJ. The mechanism of reaction of β-aryloxyacroleins with nucleosides. Chem. Res. Toxicol 1996;9:12–15. [PubMed: 8924580]
8. Dedon PC, Plastaras JP, Rouzer CA, Marnett LJ. Indirect mutagenesis by oxidative DNA damage: Formation of the pyrimidopurinone adduct of deoxyguanosine by base propenal. Proc. Natl. Acad. Sci. U.S.A 1998;95:11113–11116. [PubMed: 9736698]

9. Plastaras JP, Riggins JN, Otteneder M, Marnett LJ. Reactivity and mutagenicity of endogenous DNA oxopropenylating agents: Base propenals, malondialdehyde, and Nε-oxopropenyllysine. Chem. Res. Toxicol 2000;13:1235–1242. [PubMed: 11123964]
10. Wang MY, Liehr JG. Lipid hydroperoxide-induced endogenous DNA adducts in hamsters: Possible mechanism of lipid hydroperoxide-mediated carcinogenesis. Arch. Biochem. Biophys 1995;316:38–46. [PubMed: 7840640]
11. Chaudhary AK, Nokubo M, Reddy GR, Yeola SN, Morrow JD, Blair IA, Marnett LJ. Detection of endogenous malondialdehyde-deoxyguanosine adducts in human liver. Science 1994;265:1580–1582. [PubMed: 8079172]
12. Wang M, Dhingra K, Hittleman WN, Liehr JG, de Andrade M, Li D. Lipid peroxidation-induced putative malondialdehyde-DNA adducts in human breast tissues. Cancer Epidemiol 1996;5:705–710.
13. Nath RG, Chung FL. Detection of 1,N^2-propanodeoxyguanosine adducts in rodent and human liver DNA by ^{32}P-postlabeling. Proc. Am. Assoc. Cancer Res 1993;34:137.
14. Nath RG, Chung F-L. Detection of exocyclic 1,N^2-propanodeoxyguanosine adducts as common DNA lesions in rodents and humans. Proc. Natl. Acad. Sci. U.S.A 1994;91:7491–7495. [PubMed: 8052609]
15. O'Nair J, Barbin A, Guichard Y, Bartsch H. 1,N^6-Ethenodeoxyadenosine and 3,N^4-ethenodeoxycytidine in liver DNA from humans and untreated rodents detected by immunoaffinity/^{32}P-postlabeling. Carcinogenesis 1995;16:613–617. [PubMed: 7697821]
16. Zhang S, Villalta PW, Wang M, Hecht SS. Analysis of crotonaldehyde- and acetaldehyde-derived 1,N^2-propanodeoxyguanosine adducts in DNA from human tissues using liquid chromatography electrospray ionization tandem mass spectrometry. Chem. Res. Toxicol 2006;19:1386–1392. [PubMed: 17040109]
17. Chaudhary AK, Nokubo M, Marnett LJ, Blair IA. Analysis of the malondialdehyde-2′-deoxyguanosine adduct in rat liver DNA by gas chromatography/electron capture negative chemical ionization mass spectrometry. Biol. Mass Spectrom 1994;23:457–464. [PubMed: 7918689]
18. Rouzer CA, Chaudhary AK, Nokubo M, Ferguson DM, Reddy GR, Blair IA, Marnett LJ. Analysis of the malondialdehyde-2′-deoxyguanosine adduct pyrimidopurinone in human leukocyte DNA by gas chromatography/electron capture-negetiave chemical ionization/mass spectrometry. Chem. Res. Toxicol 1997;10:181–188. [PubMed: 9049429]
19. Vaca CE, Fang JL, Mutanen M, Valsta L. ^{32}P-postlabelling determination of DNA adducts of malonaldehyde in humans: Total white blood cells and breast tissue. Carcinogenesis 1995;16:1847–1851. [PubMed: 7634413]
20. Fang JL, Vaca CE, Valsta LM, Mutanen M. Determination of DNA adducts of malonaldehyde in humans: Effects of dietary fatty acid composition. Carcinogenesis 1996;17:1035–1040. [PubMed: 8640909]
21. Sevilla CL, Mahle NH, Eliezer N, Uzieblo A, O'Hara SM, Nokubo M, Miller R, Rouzer CA, Marnett LJ. Development of monoclonal antibodies to the malondialdehyde-deoxyguanosine adduct, pyrimidopurinone. Chem. Res. Toxicol 1997;10:172–180. [PubMed: 9049428]
22. Chaudhary AK, Reddy RG, Blair IA, Marnett LJ. Characterization of an N^6-oxopropenyl-2′-deoxyadenosine adduct in malondialdehyde-modified DNA using liquid chromatography/electrospray ionization tandem mass spectrometry. Carcinogenesis 1996;17:1167–1170. [PubMed: 8640930]
23. Hoberg AM, Otteneder M, Marnett LJ, Poulsen HE. Measurement of the malondialdehyde-2′-deoxyguanosine adduct in human urine by immuno-extraction and liquid chromatography/atmospheric pressure chemical ionization tandem mass spectrometry. J. Mass Spectrom 2004;39:38–42. [PubMed: 14760611]
24. Otteneder MB, Knutson CG, Daniels JS, Hashim M, Crews BC, Remmel RP, Wang H, Rizzo C, Marnett LJ. In vivo oxidative metabolism of a major peroxidation-derived DNA adduct, M_1dG. Proc. Natl. Acad. Sci. U.S.A 2006;103:6665–6669. [PubMed: 16614064]
25. Fink SP, Reddy GR, Marnett LJ. Mutagenicity in *Escherichia coli* of the major DNA adduct derived from the endogenous mutagen malondialdehyde. Proc. Natl. Acad. Sci. U.S.A 1997;94:8652–8657. [PubMed: 9238032]

26. VanderVeen LA, Hashim MF, Shyr Y, Marnett LJ. Induction of frameshift and base pair substitution mutations by the major DNA adduct of the endogenous carcinogen malondialdehyde. Proc. Natl. Acad. Sci. U.S.A 2003;100:14247–14252. [PubMed: 14603032]
27. Niedernhofer LJ, Daniels JS, Rouzer CA, Greene RE, Marnett LJ. Malondialdehyde, a product of lipid peroxidation, is mutagenic in human cells. J. Biol. Chem 2003;278:31426–31433. [PubMed: 12775726]
28. Mao H, Schnetz-Boutaud NC, Weisenseel JP, Marnett LJ, Stone MP. Duplex DNA catalyzes the chemical rearrangement of a malondialdehyde deoxyguanosine adduct. Proc. Natl. Acad. Sci. U.S.A 1999;96:6615–6620. [PubMed: 10359760]
29. Riggins JN, Daniels JS, Rouzer CA, Marnett LJ. Kinetic and thermodynamic analysis of the hydrolytic ring-opening of the malondialdehyde-deoxyguanosine adduct, 3-(2′-deoxy-β-d-erythro-pentofuranosyl)-pyrimido[1,2-α]purin-10(3H)-one. J. Am. Chem. Soc 2004;126:8237–8243. [PubMed: 15225065]
30. Riggins JN, Pratt DA, Voehler M, Daniels JS, Marnett LJ. Kinetics and mechanism of the general-acid-catalyzed ring-closure of the malondialdehyde-DNA adduct, N^2-(3-oxo-1-propenyl) deoxyguanosine (N^2OPdG-), to 3-(2′-deoxy-β-d-erythro-pentofuranosyl)pyrimido[1,2-α]purin-10 (3H)-one (M_1dG). J. Am. Chem. Soc 2004;126:10571–10581. [PubMed: 15327313]
31. Mao H, Reddy GR, Marnett LJ, Stone MP. Solution structure of an oligodeoxynucleotide containing the malondialdehyde deoxyguanosine adduct N^2-(3-oxo-1-propenyl)-dG (ring-opened M_1G) positioned in a $(CpG)_3$ frameshift hotspot of the *Salmonella typhimuriumhisD3052* gene. Biochemistry 1999;38:13491–13501. [PubMed: 10521256]
32. O'Hara SM, Marnett LJ. DNA sequence analysis of spontaneous and β-methoxy-acrolein-induced mutations in *Salmonella typhimuriumhisD3052*. Mutat. Res 1991;247:45–56. [PubMed: 2002804]
33. Schnetz-Boutaud NC, Saleh S, Marnett LJ, Stone MP. The exocyclic 1,N^2-deoxyguanosine pyrimidopurinone M_1G is a chemically stable DNA adduct when placed opposite a two-base deletion in the $(CpG)_3$ frameshift hotspot of the *Salmonella typhimuriumhisD3052* gene. Biochemistry 2001;40:15638–15649. [PubMed: 11747439]
34. Weisenseel JP, Moe JG, Reddy GR, Marnett LJ, Stone MP. Structure of a duplex oligodeoxynucleotide containing propanodeoxyguanosine opposite a two-base deletion in the $(CpG)_3$ frameshift hotspot of *Salmonella typhimurium* hisD3052 determined by ^{1}H NMR and restrained molecular dynamics. Biochemistry 1995;34:50–64. [PubMed: 7819223]
35. Woodson SA, Crothers DM. Preferential location of bulged guanosine internal to a G:C tract by ^{1}H NMR. Biochemistry 1988;27:436–445. [PubMed: 2964870]
36. Woodson SA, Crothers DM. Proton nuclear magnetic resonance studies on bulge-containing DNA oligonucleotides from a mutational hot-spot sequence. Biochemistry 1987;26:904–912. [PubMed: 3567151]
37. Reddy GR, Marnett LJ. Synthesis of an oligodeoxynucleotide containing the alkaline labile malondialdehyde-deoxyguanosine adduct pyrimido[1,2-a]purin-10(3H)-one. J. Am. Chem. Soc 1995;117:5007–5008.
38. Schnetz-Boutaud NC, Mao H, Stone MP, Marnett LJ. Synthesis of oligonucleotides containing the alkali-labile pyrimidopurinone adduct, M_1G. Chem. Res. Toxicol 2000;13:90–95. [PubMed: 10688532]
39. Wang H, Kozekov ID, Kozekova A, Tamura PJ, Marnett LJ, Harris TM, Rizzo CJ. Site-specific synthesis of oligonucleotides containing malondialdehyde adducts of deoxyguanosine and deoxyadenosine via a postsynthetic modification strategy. Chem. Res. Toxicol 2006;19:1467–1474. [PubMed: 17112234]
40. Cavaluzzi MJ, Borer PN. Revised UV extinction coefficients for nucleoside-5′-monophosphates and unpaired DNA and RNA. Nucleic Acids Res 2004;32:e13. [PubMed: 14722228]
41. Piotto M, Saudek V, Sklenar V. Gradient-tailored excitation for single-quantum NMR spectroscopy of aqueous solutions. J. Biomol. NMR 1992;2:661–665. [PubMed: 1490109]
42. Reid BR. Sequence-specific assignments and their use in NMR studies of DNA structure. Q. Rev. Biophys 1987;20:2–28.
43. Patel DJ, Shapiro L, Hare D. DNA and RNA: NMR studies of conformations and dynamics in solution. Q. Rev. Biophys 1987;20:35–112. [PubMed: 2448843]

44. Boelens R, Scheek RM, Dijkstra K, Kaptein R. Sequential assignment of imino- and amino-proton resonances in ^{1}H NMR spectra of oligonucleotides by two-dimensional NMR spectroscopy. Application to a *lac* operator fragment. J. Magn. Reson 1985;62:378–386.
45. Fink SP, Reddy GR, Marnett LJ. Relative contribution of cytosine deamination and error-prone replication to the induction of propanodeoxyguanosine to deoxyadenosine mutations in *Escherichia coli*. Chem. Res. Toxicol 1996;9:277–283. [PubMed: 8924603]
46. de los Santos C, Zaliznyak T, Johnson F. NMR characterization of a DNA duplex containing the major acrolein-derived deoxyguanosine adduct γ-OH-1,-N^2-propano-2′-deoxyguanosine. J. Biol. Chem 2001;276:9077–9082. [PubMed: 11054428]
47. Yang IY, Hossain M, Miller H, Khullar S, Johnson F, Grollman A, Moriya M. Responses to the major acrolein-derived deoxyguanosine adduct in *Escherichia coli*. J. Biol. Chem 2001;276:9071–9076. [PubMed: 11124950]
48. VanderVeen LA, Hashim MF, Nechev LV, Harris TM, Harris CM, Marnett LJ. Evaluation of the mutagenic potential of the principal DNA adduct of acrolein. J. Biol. Chem 2001;276:9066–9070. [PubMed: 11106660]
49. Marinelli ER, Johnson F, Iden CR, Yu PL. Synthesis of 1,N^2-(1,3-propano)-2′-deoxyguanosine and incorporation into oligodoexynucleotides: A model for exocyclic acrolein-DNA adducts. Chem. Res. Toxicol 1990;3:49–58. [PubMed: 2131825]
50. Singh US, Moe JG, Reddy GR, Weisenseel JP, Marnett LJ, Stone MP. ^{1}H NMR of an oligodeoxynucleotide containing a propanodeoxyguanosine adduct positioned in a $(CG)_3$ frameshift hotspot of *Salmonella typhimuriumhisd3052*: Hoogsteen base-pairing at pH 5.8. Chem. Res. Toxicol 1993;6:825–836. [PubMed: 8117922]
51. Moe JG, Reddy GR, Marnett LJ, Stone MP. ^{1}H NMR characterization of a duplex oligodeoxynucleotide containing propanodeoxyguanosine opposite a two-base deletion in the $(CpG)_3$ frameshift hotspot of *Salmonella typhimuriumhisD3052*. Chem. Res. Toxicol 1994;7:319–328. [PubMed: 8075363]
52. Weisenseel, JP. Ph.D. Thesis. Vanderbilt University; Nashville, TN: 2000.
53. Weisenseel JP, Reddy GR, Marnett LJ, Stone MP. Structure of the 1,N^2-propanodeoxyguanosine adduct in a three-base DNA hairpin loop derived from a palindrome in the *Salmonella typhimuriumhisD3052* gene. Chem. Res. Toxicol 2002;15:140–152. [PubMed: 11849039]
54. Weisenseel JP, Reddy GR, Marnett LJ, Stone MP. Structure of an oligodeoxynucleotide containing a 1,N^2-propanodeoxyguanosine adduct positioned in a palindrome derived from the *Salmonella typhimuriumhisD3052* gene: Hoogsteen pairing at pH 5.2. Chem. Res. Toxicol 2002;15:127–139. [PubMed: 11849038]
55. Kouchakdjian M, Marinelli E, Gao X, Johnson F, Grollman A, Patel D. NMR studies of exocyclic 1,N^2-propanodeoxyguanosine adducts (X) opposite purines in DNA duplexes: Protonated X(syn):A (anti) pairing (acidic pH) and X(syn):G(anti) pairing (neutral pH) at the lesion site. Biochemistry 1989;28:5647–5657. [PubMed: 2775729]
56. Kouchakdjian M, Eisenberg M, Live D, Marinelli E, Grollman AP, Patel DJ. NMR studies of an exocyclic 1N^2-propanodeoxyguanosine adduct (X) located opposite deoxyadenosine (A) in DNA duplexes at basic pH: Simultaneous partial intercalation of X and A between stacked bases. Biochemistry 1990;29:4456–4465. [PubMed: 2161685]
57. Huang P, Eisenberg M. The three-dimensional structure in solution (pH 5.8) of a DNA 9-mer duplex containing 1,N^2-propanodeoxyguanosine opposite deoxyadenosine. Restrained molecular dynamics and NOE-based refinement calculations. Biochemistry 1992;31:6518–6532. [PubMed: 1633163]
58. Huang P, Patel DJ, Eisenberg M. Solution structure of the exocyclic 1,N^2-propanodeoxyguanosine adduct opposite deoxyadenosine in a DNA nonamer duplex at pH 8.9. Model of pH-dependent conformational transition. Biochemistry 1993;32:3852–3866. [PubMed: 8385990]
59. Plum GE, Grollman AP, Johnson F, Breslauer KJ. Influence of an exocyclic guanine adduct on the thermal stability, conformation, and melting thermodynamics of a DNA duplex. Biochemistry 1992;31:12096–12102. [PubMed: 1457406]
60. Streisinger G, Okada Y, Enrich J, Newton J, Tsugita A, Terzaghi E, Inouye M. Frameshift mutations and the genetic code. Cold Spring Harbor Symp. Quant. Biol 1966;31:77–84. [PubMed: 5237214]

61. Hartman PE, Ames BN, Roth JR, Barnes WM, Levin DE. Target sequences for mutagenesis in *Salmonella* histidine-requiring mutants. Environ. Mutagen 1986;8:631–641. [PubMed: 3525139]
62. Oeschger NS, Hartman PE. ICR-induced frameshift mutations in histidine operon of *Salmonella*. J. Bacteriol 1970;101:490–504. [PubMed: 4905310]
63. McCann J, Spingarn NE, Koburi J, Ames BN. Detection of carcinogens as mutagens: Bacterial tester strains with R-factor plasmids. Proc. Natl. Acad. Sci. U.S.A 1975;72:979–983. [PubMed: 165497]
64. DeMarini DM, Abu-Shakra A, Gupta R, Hendee LJ, Levine JG. Molecular analysis of mutations induced by the intercalating agent ellipticine at the *hisD3052* allele of *Salmonella typhimurium* TA98. Environ. Mol. Mutagen 1992;20:12–18. [PubMed: 1639078]
65. Bell DA, Levine JG, DeMarini DM. DNA sequence analysis of revertants of the hisD3052 allele of *Salmonella typhimurim* TA98 using the polymerase chain reaction and direct sequencing: Application to 1-nitropyrene-induced revertants. Mutat. Res 1991;252:35–44. [PubMed: 1996130]
66. Fuscoe JC, Wu R, Shen NH, Healy SK, Felton JS. Change analysis of revertants of the *hisD3052* allele in *Salmonella typhimurium*. Mutat. Res 1988;201:241–251. [PubMed: 3138534]
67. Isono K, Yourno J. Chemical carcinogens as frameshift mutagens: *Salmonella* DNA sequence sensitive to mutagenesis by polycyclic carcinogens. Proc. Natl. Acad. Sci. U.S.A 1974;71:1612–1617. [PubMed: 4525453]
68. Patel DJ, Kozlowski SA, Marky LA, Rice JA, Broka C, Itakura K, Breslauer KJ. Extra adenosine stacks into the self-complementary d(CGCAGAATTCGCG) duplex in solution. Biochemistry 1982;21:445–451. [PubMed: 7066296]
69. Morden KM, Chu YG, Martin FH Jr. Unpaired cytosine in the deoxyoligonucleotide duplex dCA_3CA_3G:dCT_6G is outside of the helix. Biochemistry 1983;22:5557–5563.
70. Morden KM, Gunn BM, Maskos K. NMR studies of a deoxyribodecanucleotide containing an extrahelical thymidine surrounded by an oligo(dA):oligo(dT) tract. Biochemistry 1990;29:8835–8845. [PubMed: 2271560]
71. Rosen MA, Live D, Patel DJ. Comparative NMR study of An-bulge loops in DNA duplexes: Intrahelical stacking of A, A-A, and A-A-A bulge loops. Biochemistry 1992;31:4004–4014. [PubMed: 1314654]
72. Rosen MA, Shapiro L, Patel DJ. Solution structure of a trinucleotide A-T-A bulge loop within a DNA duplex. Biochemistry 1992;31:4015–4026. [PubMed: 1314655]
73. Joshua-Tor L, Frolow F, Appella E, Hope H, Rabinovich D, Sussman JL. Three-dimensional structures of bulge-containing DNA fragments. J. Mol. Biol 1992;225:397–431. [PubMed: 1593627]
74. Morden KM, Maskos K. NMR studies of an extrahelical cytosine in an A•T rich region of a deoxyribodecanucleotide. Biopolymers 1993;33:27–36. [PubMed: 8427936]
75. Aboul-ela F, Murchie AI, Homans SW, Lilley DM. Nuclear magnetic resonance study of deoxyoligonucleotide duplex containing a three base bulge. J. Mol. Biol 1993;229:173–188. [PubMed: 8380616]
76. Patel DJ, Kozlowski SA, Ikuta S, Itakura K, Bhatt R, Hare DR. NMR studies of DNA conformation and dynamics in solution. Cold Spring Harbor Symp. Quant. Biol 1982;97:197–206.
77. Nikonowicz EP, Meadows RP, Gorenstein DG. NMR structural refinement of an extrahelical adenosine tridecamer $d(CGCAGAATTCGCG)_2$ via a hybrid relaxation matrix procedure. Biochemistry 1990;29:4193–4204. [PubMed: 2361138]
78. van den Hoogen YT, van Beuzekom AA, de Vroom E, Van Der Marel GA, van Boom JH, Altona C. Bulge-out structures in the single-stranded trimer AUA and in the duplex (CUGGUGCGG):(CCGCCCAG). A model-building and NMR study. Nucleic Acids Res 1988;16:5013–5030. [PubMed: 3387215]
79. van den Hoogen YT, van Beuzekom AA, van den Elst H, van der Marel GA, van Boom JH, Altona C. Extra thymidine stacks into the d(CTGGTGCGG):d(CCGCCCAG) duplex. An NMR and model-building study. Nucleic Acids Res 1988;16:2971–2986. [PubMed: 3368313]
80. Kalnik MW, Norman DG, Li BF, Swann PF, Patel DJ. Conformational transitions in thymidine bulge-containing deoxytridecanucleotide duplexes: Role of flanking sequence and temperature in modulating the equilibrium between looped out and stacked thymidine bulge states. J. Biol. Chem 1990;265:636–647. [PubMed: 2295611]

81. Maskos K, Gunn BM, LeBlanc DA, Morden KM. NMR study of G•A and A•A pairing in $(dGCGAATAAGCG)_2$. Biochemistry 1993;32:3583–3595. [PubMed: 8385483]
82. Bebenek K, Kunkel TA. Streisinger revisited: DNA synthesis errors mediated by substrate misalignments. Cold Spring Harbor Symp. Quant. Biol 2000;65:81–91. [PubMed: 12760023]
83. Benamira M, Singh U, Marnett LJ. Site-specific frameshift mutagenesis by a propanodeoxyguanosine adduct positioned in the $(CpG)_4$ hot-spot of *Salmonella typhimuriumhisD3052* carried on an M13 vector. J. Biol. Chem 1992;267:22392–22400. [PubMed: 1429591]
84. Tippin B, Kobayashi S, Bertram JG, Goodman MF. To slip or skip, visualizing frameshift mutation dynamics for error-prone DNA polymerases. J. Biol. Chem 2004;279:45360–45368. [PubMed: 15339923]
85. Hashim MF, Riggins JN, Schnetz-Boutaud N, Voehler M, Stone MP, Marnett LJ. *In vitro* bypass of malondialdehyde-deoxyguanosine adducts: Differential base selection during extension by the Klenow fragment of DNA polymerase I is the critical determinant of replication outcome. Biochemistry 2004;43:11828–11835. [PubMed: 15362868]
86. Tippin B, Pham P, Goodman MF. Error-prone replication for better or worse. Trends Microbiol 2004;12:288–295. [PubMed: 15165607]
87. Prakash S, Johnson RE, Prakash L. Eukaryotic translesion synthesis DNA polymerases: Specificity of structure and function. Annu. Rev. Biochem 2005;74:317–353. [PubMed: 15952890]
88. Zang H, Goodenough AK, Choi JY, Irimia A, Loukachevitch LV, Kozekov ID, Angel KC, Rizzo CJ, Egli M, Guengerich FP. DNA adduct bypass polymerization by *Sulfolobus solfataricus* DNA polymerase Dpo4. Analysis and crystal structures of multiple base-pair substitution and frameshift products with the adduct 1,N^2-ethenoguanine. J. Biol. Chem 2005;280:29750–29764. [PubMed: 15965231]
89. Irimia A, Zang H, Loukachevitch LV, Eoff RL, Guengerich FP, Egli M. Calcium is a cofactor of polymerization but inhibits pyrophosphorolysis by the *Sulfolobus solfataricus* DNA polymerase Dpo4. Biochemistry 2006;45:5949–5956. [PubMed: 16681366]

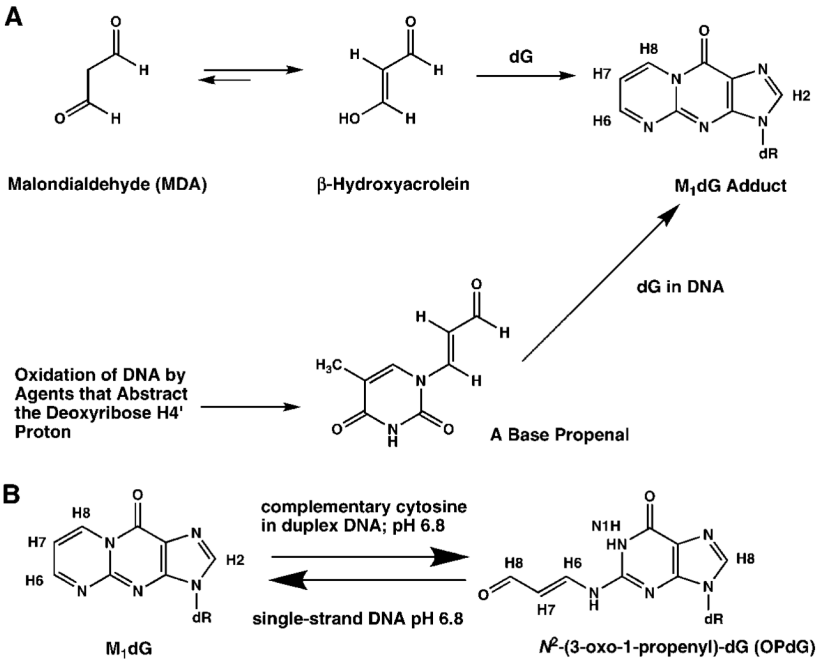

[a] In panel A, thymine propenal is shown as a representative base propenal. Note the numbering scheme for M_1dG in which the imidazole proton is H2, corresponding to the H8 proton in purines. The exocyclic ring protons are numbered H6, H7, and H8. In panel B, in duplex DNA when M_1dG is placed opposite dC, it is quantitatively converted to N^2-(3-oxo-1-propenyl)dG, the OPdG adduct.

Scheme 1.

(A) Formation of M_1dG from MDA or from Base Propenals and (B) Depiction of M_1dG Being Stable in Single-Stranded DNA [a]

$$\begin{array}{l} 5'\text{-}A^{-2}T^{-1}C^{1}\ G^{2}\ C^{3}\ X^{4}\ C^{5}\ G^{6}\ G^{7}\ C^{8}\ A^{9}\ T^{10}G^{11}\text{-}3' \\ 3'\text{-}T^{22}A^{21}G^{20}C^{19}G^{18} \qquad\quad C^{17}C^{16}G^{15}T^{14}A^{13}C^{12}\text{-}5' \end{array}$$

[a] Named the M_1dG-2BD oligodeoxynucleotide when X = M_1dG and named the OPdG-2BD oligodeoxynucleotide when X = OPdG. The position of the two-base bulge is indicated as for the M_1dG-2BD oligodeoxynucleotide, i.e., consisting of M_1dG and the 3′-neighbor dC (*33*). For the unmodified 2BD duplex and for the OPdG-2BD oligodeoxynucleotide, the position of the bulge migrates on the NMR time scale (see the text). The nucleotide numbering scheme is derived so that it is consistent with previous studies on this iterated repeat sequence from the *hisD3052* gene (*51*).

Scheme 2.

2BD Oligodeoxynucleotide Duplex Containing a Two-Nucleotide 5′-GpC-3′ Deletion in the Complementary Strand [a]

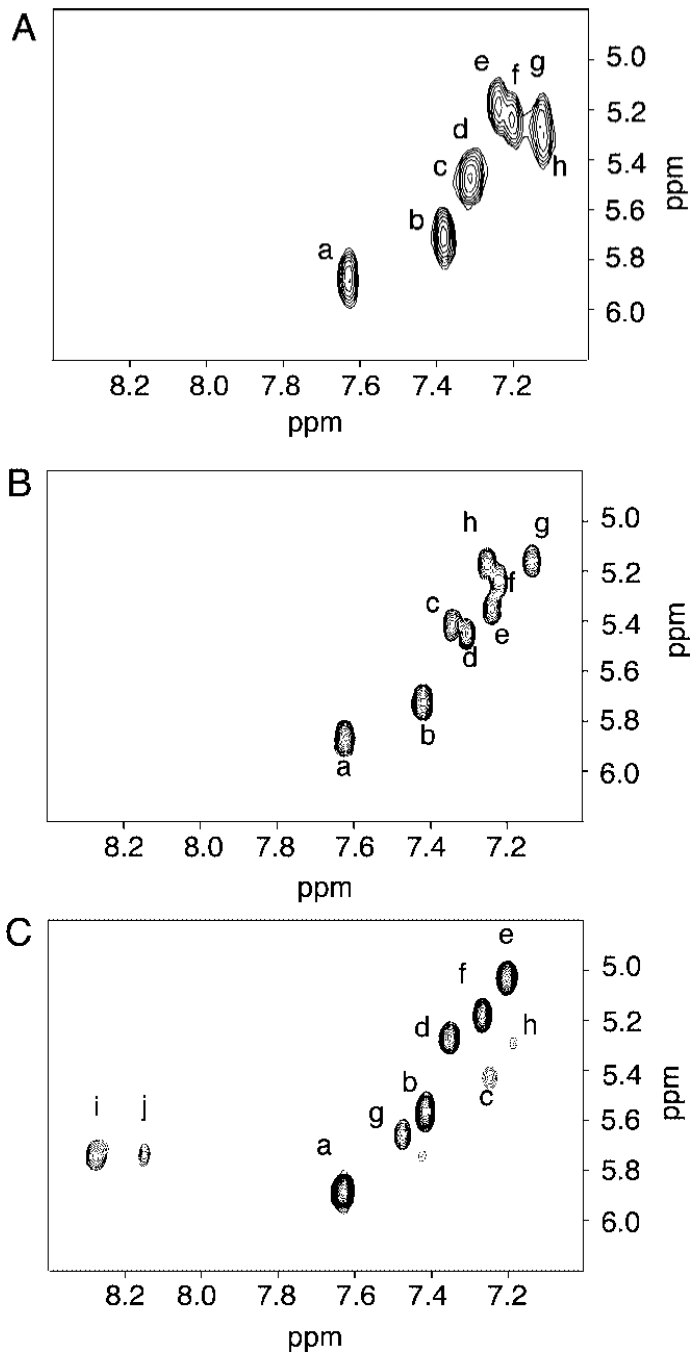

Figure 1.

(A) COSY spectrum of the unmodified 2BD duplex. (B) COSY spectrum of the freshly prepared OPdG-2BD duplex. (C) COSY spectrum of the freshly prepared M_1dG-2BD duplex. Cross-peaks: a, C^{12} H5 → C^{12} H6; b, C^1 H5 → C^1 H6; c, C^3 H5 → C^3 H6; d, C^{17} H5 → C^{17} H6; e, C^{16} H5 → C^{16} H6; f, C^8 H5 → C^8 H6; g, C^5 H5 → C^5 H6; h, C^{19} H5 → C^{19} H6; i, M_1dG H7 → H8; j, M_1dG H6 → H7. The experiments were performed at 800 MHz and 25 °C.

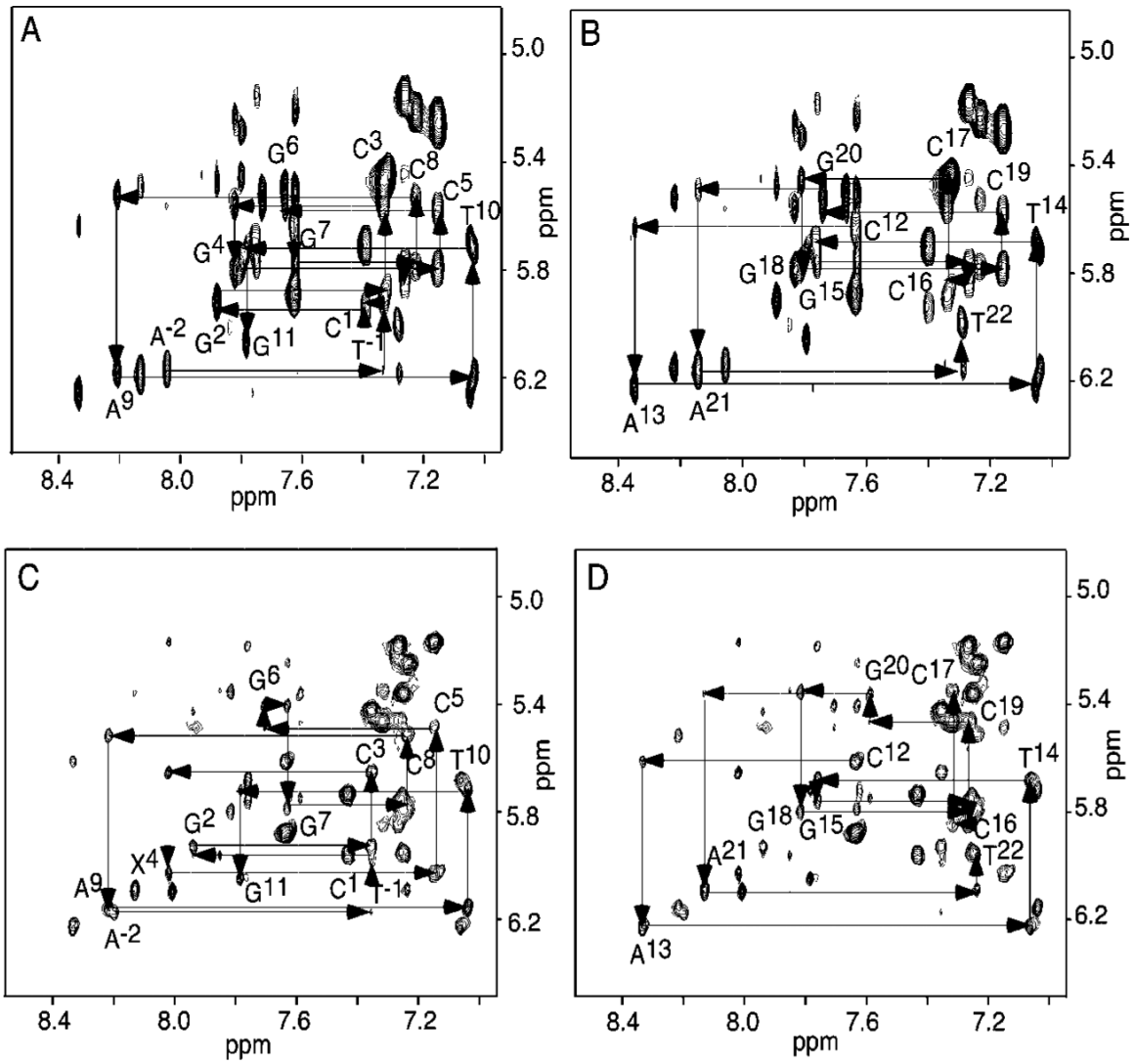

Figure 2.

(A) Expanded plot showing sequential NOE connectivity between aromatic and anomeric protons for nucleotides $A^{-2} \rightarrow G^{11}$ of the unmodified 2BD duplex. (B) Expanded plot showing sequential NOE connectivity between aromatic and anomeric protons for nucleotides $C^{12} \rightarrow T^{22}$ of the unmodified 2BD duplex. (C) Expanded plot showing sequential NOE connectivity between aromatic and anomeric protons for nucleotides $A^{-2} \rightarrow G^{11}$ of the OPdG-2BD duplex. (D) Expanded plot showing sequential NOE connectivity between aromatic and anomeric protons for nucleotides $C^{12} \rightarrow T^{22}$ of the OPdG-2BD duplex. The 800 MHz 250 ms mixing time NOESY experiments were conducted at 25 °C.

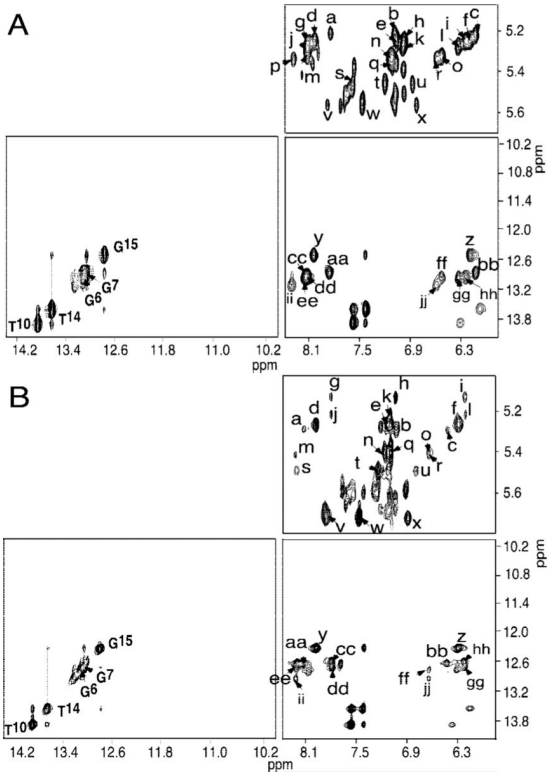

Figure 3.

(A) Expanded plot showing sequential NOE connectivity of the base-paired imino protons for the unmodified 2BD duplex. (B) Expanded plot showing sequential NOE connectivity for the base-paired imino protons of the freshly prepared OPdG-2BD duplex. Cross-peaks: a, C^{16} N^4H2 → C^{16} H5; b, C^{16} H6 → C^{16} H5; c, C^{16} N^4H1 → C^{16} H5; d, C^8 N^4H2 → C^8 H5; e, C^8 H6 → C^8 H5; f, C^8 N^4H1 → C^8 H5; g, C^5 N^4H2 → C^5 H5; h, C^5 H6 → C^5 H5; i, C^5 N^4H1 → C^5 H5; j, C^{19} N^4H2 → C^{19} H5; k, C^{19} H6 → C^{19} H5; l, C^{19} N^4H1 → C^{19} H5; m, C^{17} N^4H2 → C^{17} H5; n, C^{17} H6 → C^{17} H5; o, C^{17} N^4H1 → C^{17} H5; p, C^3 N^4H2 → C^3 H5; q, C^3 H6 → C^3 H5; r, C^3 N^4H1 → C^3 H5; s, C^1 N^4H2 → C^1 H5; t, C^1 H6 → C^1 H5; u, C^1 N^4H1 → C^1 H5; v, C^{12} N^4H2 → C^{12} H5; w, C^{12} H6 → C^{12} H5; x, C^{12} N^4H1 → C^{12} H5; y, G^{15} N1H → C^8 N^4H2; z, G^{15} N1H → C^8 N^4H1; aa, G^7 N1H → C^{16} N^4H2; bb, G^7 N1H → C^{16} N^4H1; cc, G^{18} N1H → C^5 N^4H2; dd, G^2 N1H and X^4 N1H → C^{19} N^4H2; ee, G^6 N1H and X^4 N1H → C^{17} N^4H2; ff, G^{18} N1H → C^5 N^4H1; gg, G^2 N1H and X^4 N1H → C^{19} N^4H1; hh, G^6 N1H and X^4 N1H → C^{17} N^4H1; ii, G^{18} N1H and G^{20} N1H → C^3 N^4H2; jj, G^{18} N1H and G^{20} N1H → C^3 N^4H1. The 800 MHz, 250 ms mixing time NOESY experiments were performed at 10 °C.

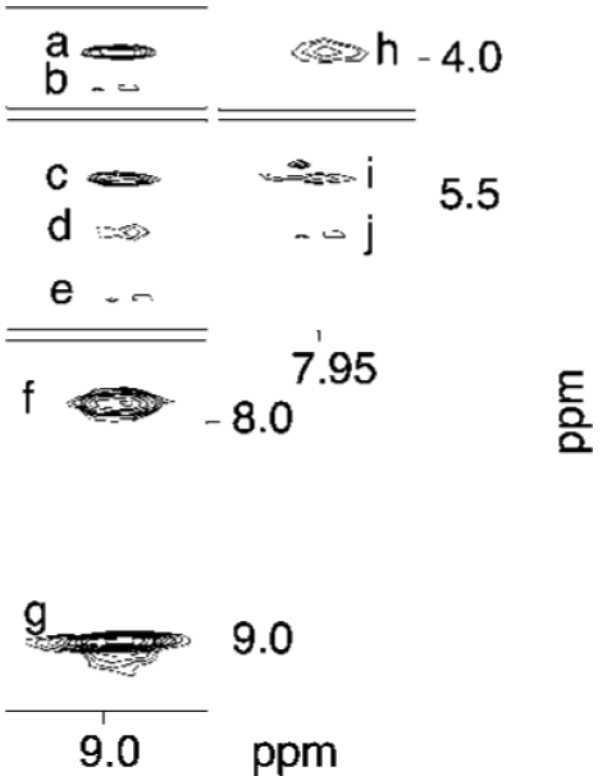

Figure 4.
Tile plot showing NOE cross-peaks between OPdG protons and DNA protons in the OPdG-2BD duplex. Cross-peaks: a, OPdG H8 → C^5 H5′; b, OPdG H8 → C^5 H4′; c, OPdG H8 → C^5 H1′; d, OPdG H8 → OpdG H6; e, OPdG H8 → X^4 H1′; f, OPdG H8 → OPdG H7; g, OPdG H8 → OPdG H8; h, OPdG H7 → C^5 H5′; i, OPdG H7 → C^5 H1′; j, OPdG H7 → OPdG H6. The 800 MHz, 250 ms mixing time NOESY experiment was conducted at 25 °C.

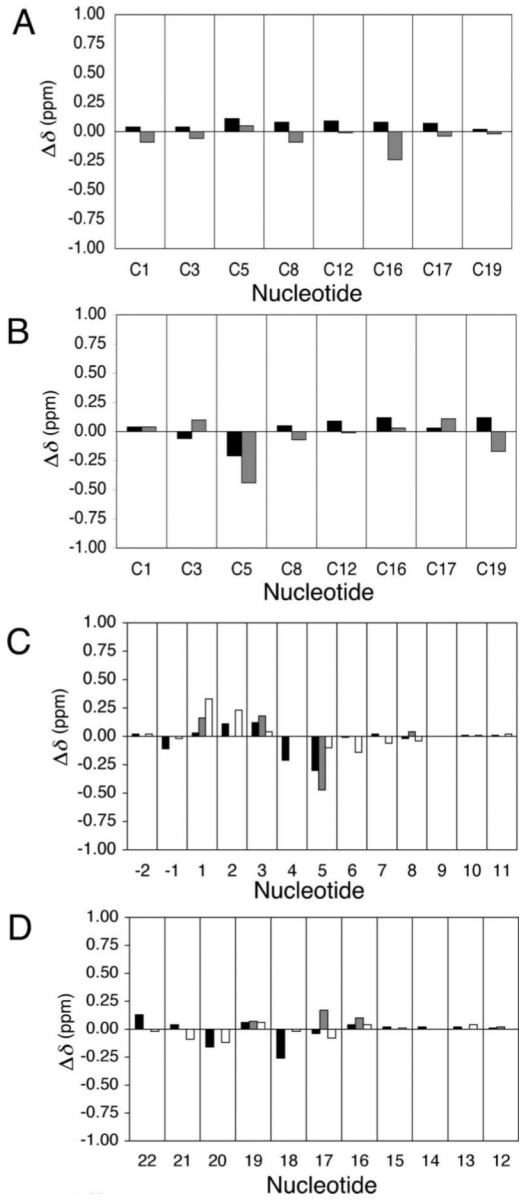

Figure 5.

(A) Chemical shift differences of cytosine H5 and H6 protons of the OPdG-2BD duplex relative to the unmodified 2BD duplex. (B) Chemical shift differences of cytosine H5 and H6 protons of the M_1dG-2BD duplex relative to the unmodified 2BD duplex. The data for the cytosine H5 protons are colored gray and the data for the cytosine H6 protons black. (C) Chemical shift differences of nucleotide base protons $A^{-2} \rightarrow G^{11}$ of the OPdG-2BD duplex relative to the M_1dG-2BD duplex. (D) Chemical shift differences of nucleotide base protons $C^{12} \rightarrow T^{22}$ of the OPdG-2BD duplex relative to the M_1dG-2BD duplex. The data for the nucleotide base aromatic H8/H6 protons are colored black, the data for the cytosine aromatic H5 protons gray, and the data for the sugar H1′ protons white. In all instances, $\Delta\delta = \delta_{\text{modified oligodeoxynucleotide}} - \delta_{\text{unmodified oligodeoxynucleotide}}$ (parts per million).

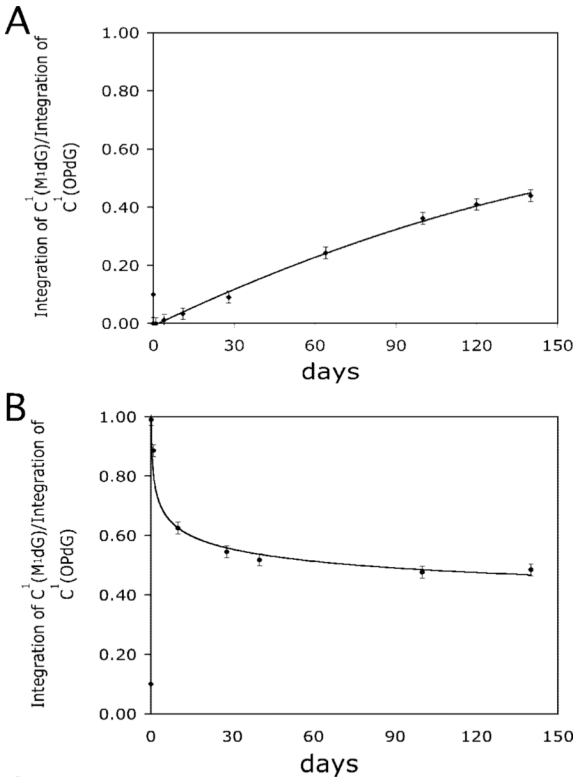

Figure 6.

Intensity ratios of the two C^1 H5 → C^1 H6 cross-peaks in the COSY spectrum, arising from M_1dG and OPdG, as a function of time: (A) freshly prepared OpdG-2BD duplex and (B) freshly prepared M_1dG-2BD duplex. The solid lines represent the best fits through the data in both plots. The errors in measuring the ratios are estimated to be ±2%.